Synthesis of carbon nanocoil forests on BaSrTiO₃ substrates with the aid of a Sn catalyst

Jingyu Sun, Antal A. Koós, Frank Dillon, Kerstin Jurkschat, Martin R. Castell, Nicole Grobert *

University of Oxford, Department of Materials, Parks Road, Oxford OX1 3PH, UK

ARTICLE INFO

ABSTRACT

A simple route for the Sn-assisted synthesis of carbon nanocoils (CNCs) by chemical vapor deposition of acetylene on polycrystalline BaSrTiO₃ (BST) substrates is reported. In this study, high-quality CNC forests have been synthesized on BST substrates with the presence of Sn. The morphologies and qualities of the CNCs were characterized by scanning electron microscopy, transmission electron microscopy, and Raman spectroscopy, while the structures and compositions of catalysts were investigated by transmission electron microscopy and energy-dispersive X-ray spectroscopy. Structural control over the CNCs was achieved by simply altering the Sn concentration or acetylene flow rates. This study demonstrates that Sn can act as an efficient catalyst for CNC synthesis in conjunction with either perovskite oxides (BST) or transition metals (Fe).

1. Introduction

Research in the field of helical carbon nanostructures has grown rapidly in the past decade, owing to their unique morphologies and attractive properties [1,2]. These nanostructures have generally been referred to as carbon nanocoils (CNCs), and have been investigated for implementation in numerous applications, for instance in structural cushions (nanosprings) [3], field emission displays [4,5], and as magnetic components [6]. To fulfil the rational use of helical carbons, various approaches towards synthesis have been attempted to gain control over the structures and hence the properties of the products.

Chemical vapor deposition (CVD) is the most commonly used synthesis technique for CNCs and the catalyst material employed within the CVD reactions plays a crucial role [4,7,8]. It was shown that the size, shape, and yield of the grown nanostructures are governed by the chemical and geometrical features of the catalyst [8–10]. To date, assorted types of catalysts have been investigated for the formation of CNCs, which mainly include Cu [7,8], Fe/Sn [11,12], Fe/In [12,13], TiC [14] and alkali compounds [4,15]. Based on these studies, several growth models have been proposed in the literature; the prevailing mechanism is based on the anisotropic extrusion of carbon from different facets/sites of catalyst particles, which is attributed to catalyst topography [7,8,16] as well as inhomogeneity of chemical composition within a particle [14,17].

Amongst the metal catalysts used in the growth of CNCs, Sn has attracted most attention owing to its capacity to lead to efficient synthesis of carbon coils at low cost. Unlike transition metal catalysts (*i.e.* Fe, Ni), Sn de-wets the graphite nanostructure surfaces and thus promotes non-linear growth of carbon [12]. Sn has been extensively reported as cooperating with Fe and/or Fe–In in synthesizing CNCs. However, to some extent, these investigations suffered from either tedious catalyst preparation procedures or low selectivity of CNC products, and also did not generate high-quality CNC

forests [11,17,18], which have been shown to have great potential for various applications such as nanoelectromechanical systems and field emissions [4,12,19].

Herein we report Sn-assisted synthesis of high-purity/selectivity CNCs on polycrystalline $BaSrTiO_3$ (BST) substrates by acetylene (C_2H_2)-CVD, and demonstrate, for the first time, CNC forest growth on perovskite oxides. Previous research has indicated that BST may be a good candidate for numerous applications, e.g. high-sensitivity sensors and tunable microwave systems, owing to the benefits of its low cost and well-known ferroelectric properties [20,21]. The combination of the CNC with BST may create new properties and lead to the fabrication of future MEMS-based devices [21]. The synthesis of high-quality CNC forests on perovskite substrates, BST, has been achieved by using Sn–Fe binary catalysts. Structural control over the grown product was achieved by simply altering the Sn concentrations or C_2H_2 flow rates.

2. Experimental

2.1. Catalyst fabrication

Epi-polished (one-sided) polycrystalline $BaSrTiO_3$ substrates (PI-KEM Ltd., UK) were employed in this work. The as-received substrates were used for CVD reactions, without any further treatment. As-received substrates were used because it was found that they contained small amounts of Sn within the pits (grain boundary triple junctions) of the BST surface; Sn was introduced by the manufacturer when the substrates were positioned on a Sn plate for polishing. Subsequently, the samples were processed using water-based, chemical–mechanical planarization steps, thus it is likely that the Sn is completely removed from the sample surfaces, but remains inside the pits as residues (see Supplementary Information Fig. S1).

The BHF-etched substrates were prepared in order to control the Sn concentration coated on BST substrates. The as-received BST substrates were etched for 5 min in a buffered NH_4F–HF solution (BHF) of pH 4.5 according to the recipe described by Kawasaki et al. [22] to remove any possible metal contamination. $SnCl_2$ powders (Sigma–Aldrich Co. LLC, UK) were used and mixed with ethanol to prepare four solutions with different Sn^{2+} concentrations ($c(Sn^{2+}) \sim 0.01/0.03/0.06/0.1$ mol/L), which are shown to have a critical effect on the structural changes on the grown CNC product (Section 3.2.3). The etched samples were coated with Sn by simply dipping them into the Sn^{2+} solutions. The Sn-coated samples were then dipped into a ferrocene-ethanol solution ($c(Fe^{2+})$ - ~ 0.02 mol/L) for 5 s, to provide sufficient Fe catalysts for CNC growth.

2.2. Carbon nanocoil synthesis

CNCs were produced using an atmospheric CVD system. BST substrates were placed inside a quartz tube (2.2 cm inner diameter) which was then positioned in a 50 cm long horizontal electrical tube furnace. C_2H_2 was used as carbon feedstock and was delivered at a flow rate of 20–40 standard cubic centimeters per minute (sccm) during the growth stage. CVD reactions were performed at 750 °C in mixtures of 900 sccm Ar and 100 sccm H_2 for 15 min, with a H_2 pretreatment at 750 °C (800 sccm, 5 min) prior to the introduction of C_2H_2. During heating and cooling the system was flushed with 200 sccm Ar. The resultant material-covered substrates were then collected for characterization. No purification procedures were used.

2.3. Characterization

The morphology of the grown CNCs was analyzed by using a JEOL JSM 840F scanning electron microscope (SEM) working at 5 kV, and a JEOL JEM 4000HR transmission electron microscope (TEM) operating at an acceleration voltage of 80 kV. The quality of obtained CNCs was inspected by Raman spectroscopy (JY Horiba Labram Aramis confocal Raman microscope with a 532 nm doubled Nd:YAG laser). Elemental analysis for the grown samples was performed by using energy-dispersive X-ray spectroscopy (EDX) equipped within a JEOL JSM 840A SEM and a JEOL JEM 2010 TEM, and a G Clam X-ray photoelectron spectrometer (XPS) with X-ray radiation from the Mg Kα band (hυ = 1253 eV).

3. Results

3.1. Synthesis of CNCs on as-received $BaSrTiO_3$ substrates

SEM-EDX characterization of as-received BST substrate surfaces (Fig. S1) confirmed that Sn was located inside the pits of the substrate; there is no trace of Sn at the polished, flat surfaces of the substrate. Moreover, there were no other metals found either within the pit or at the substrate surface. The SEM–EDX measurements reveal that the pits on the BST substrates are perfect sites to accommodate Sn-residues, which would be beneficial to the growth of CNCs, as discussed below.

Investigations of the growth temperature effect on CNC synthesis on as-received substrates (Fig. S2) indicated that 750 °C was the optimum. CNCs synthesized on the as-received BST substrates at 750 °C by C_2H_2-CVD (C_2H_2 flow rate: 40 sccm) are shown in Fig. 1. CNC selectivity (the ratio of the CNC to the entire carbon fiber amount) was obtained by counting the numbers of CNCs from numerous SEM images. It can be observed that clusters of CNCs uniformly sprout from the pits on the substrate, in large quantities and with high CNC selectivity (ca. 91%). The low-magnification SEM image (Fig. 1a) shows a general view of the BST substrate surface after the CVD reaction. It is worth noting that the pits on the surface function as the cultivating centers for 'nurturing' the growth of CNC clusters, as indicated by the white arrows marked on the image. The grown CNC clusters have a measured areal density of $\sim 2 \times 10^5$/cm². Fig. 1b shows a closer view of these CNC clusters, within which are contained branches of CNCs with different coil diameters and pitches. An individual coil is representatively displayed in the inset of Fig. 1c. More detailed characterizations of these obtained CNCs with diversified shapes are shown in the high-resolution SEM image library in Fig. S3.
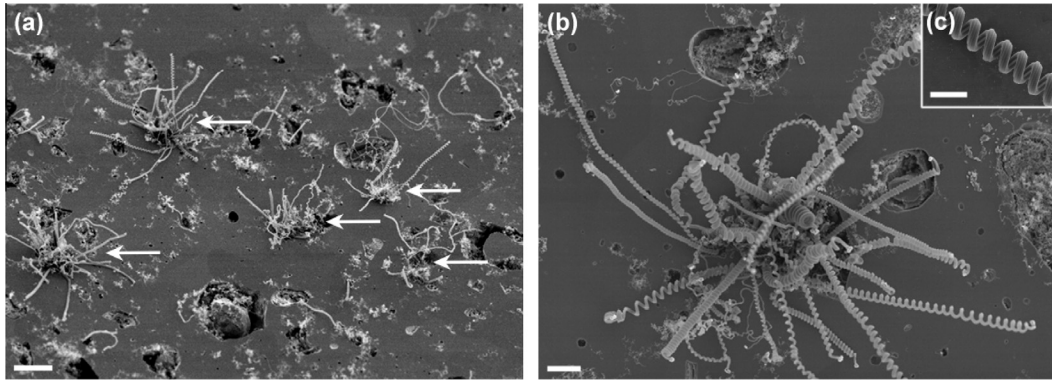
Fig. 1 – SEM images of CNCs grown on as-received BST substrates. Scale bars: (a) 5 μm. (b) 3 μm. (c) 1 μm.

The coiled nanostructures obtained were further investigated by SEM, TEM and Raman spectroscopy. For comparison, similar sizes and shapes of grown CNCs are shown in the SEM images (Fig. 2a–c) and in the TEM micrographs (Fig. 2d–f). The TEM observation reveals that the CNCs differ from each other in coil diameters (range: 200–900 nm) and lengths of pitches (range: 200–600 nm), which originates from the inhomogeneous size and shape distributions of catalyst particles, since the sizes and geometries of catalyst particles can dictate the morphologies and scales of resultant carbon nanostructures. Moreover, it can be seen from the TEM images that the CNCs barely possess hollow channels along the axis of the tubules, from which the helical structures are formed, therefore indicating that the structures of these CNCs are similar to carbon nanofibers (CNFs). The representative Raman spectrum of grown CNCs (Fig. 2g) exhibits the characteristic D and G
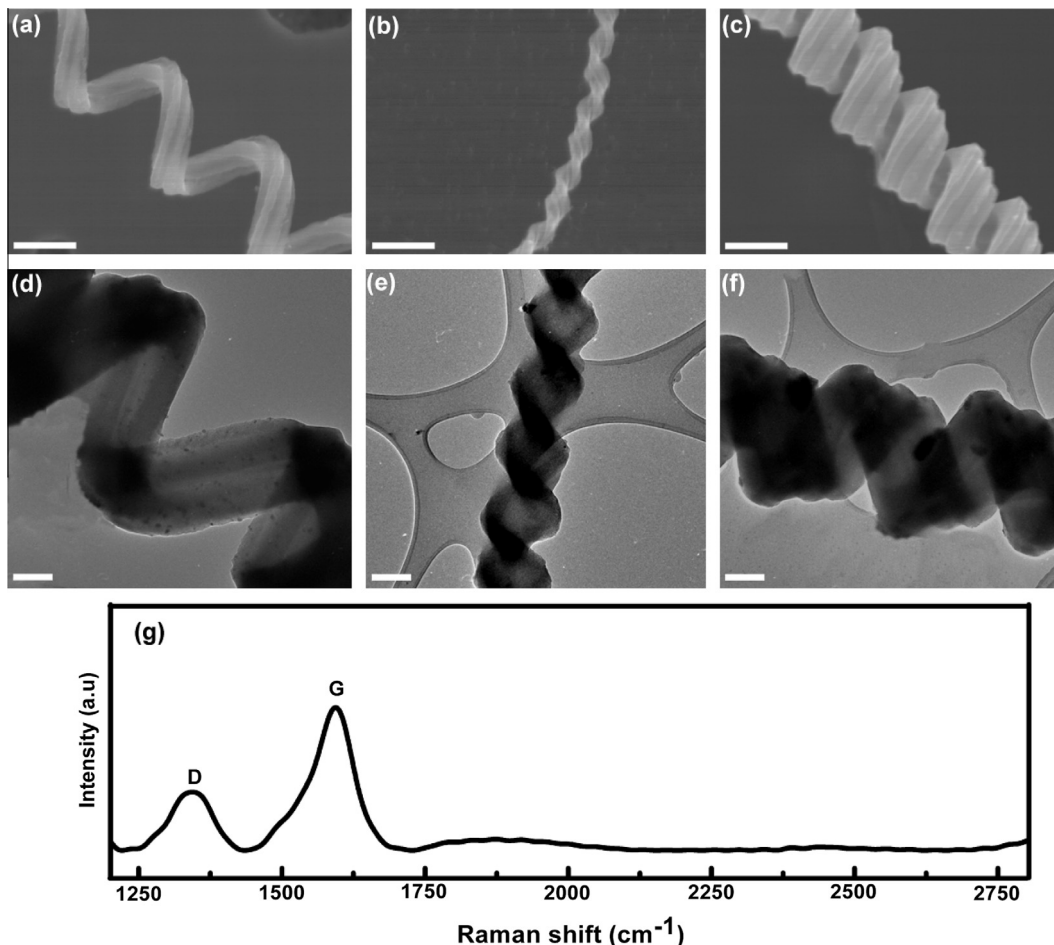
Fig. 2 – Detailed characterization of CNCs grown on as-received BST substrates. (a–c) SEM images of distinct shaped-CNCs. Scale bars: 500 nm. (d–f) TEM observations of CNCs in similar sizes and shapes as shown in SEM images (a–c), respectively. Scale bars: 200 nm. (g) A representative Raman spectrum of grown CNCs showing the characteristic D and G peaks.

peaks, with a G/D ratio at approx. 2.2, indicating a fairly high graphitization of CNCs.

Fig. 3a presents a cross-sectional SEM view of CNCs grown from a specific pit on the as-received substrate, where it can be seen that the catalyst particles locate at the tips of the grown CNCs. The tip growth mode of synthesized CNCs is consistent with that previously reported [9,12,17,23], and is due to the weak interactions between the catalyst particles and the substrate surfaces. Further characterization of the grown sample was performed with the aid of point-localized EDX equipped within a TEM, which reveals the detailed chemical constitutions of catalyst particles. Fig. 3b shows a representative TEM micrograph of the CNC, with a catalyst particle located at the tip. This inspected nanocoil possesses a diameter of approx. 600 nm and a pitch length of approx. 200 nm. The catalyst particle trapped at the tip of the nanocoil appears to have an irregular polyhedral structure. Fig. 3c shows a point-localized EDX spectrum of the catalyst particle, which displays that the TEM–EDX signal from the catalyst particle mainly consists of Sn, Sr, Ba, Ti, and O. The quantitative EDX analysis on the catalyst particle reveals that the molar ratio of (Sn:Ba:Sr:Ti:O) is approximately 0.1:0.6:0.4:1:3 ($Sn/Ba_{0.6}Sr_{0.4}TiO_3$ NPs), Herein Sn is regarded as being critical for the efficient synthesis of CNCs (See

Fig. 4 for comparison), the source of which originates from the Sn-residues trapped inside the pits of the as-received BST substrates.

The results shown in Fig. 3 also suggest that BST also played an important catalytic role, other than just being a catalyst support. It is reasonable to investigate whether BST remains catalytically active in the formation of CNCs when no Sn is present. To achieve this, we have performed metal-free CVD experiments using scratched BHF-etched BST substrates (Fig. S4). Interestingly, CNCs were obtained on such substrates, although they were produced under restricted reaction conditions and with limited yields, as depicted in Fig. 4. Fig. 4a and b present the structures of carbon solenoids, which were occasionally observed on the scratched surfaces after a CVD reaction at 750 °C. A higher magnification SEM micrograph of Fig. 4b is shown in Fig. 4c, where the white arrow marked on the image points to a catalyst particle. The EDX spectrum generated from the white box in Fig. 4b is displayed in Fig. 4e, showing the presence of Ba, Sr, Ti, O, and C. The grown samples were also subject to XPS characterization (Fig. 4d), which indicates that the sample surface is free of metals. This demonstrates (i) that BST on its own is catalytically active in the formation of CNCs and (ii) that CNC growth without Sn results in a much lower yield of target products. In
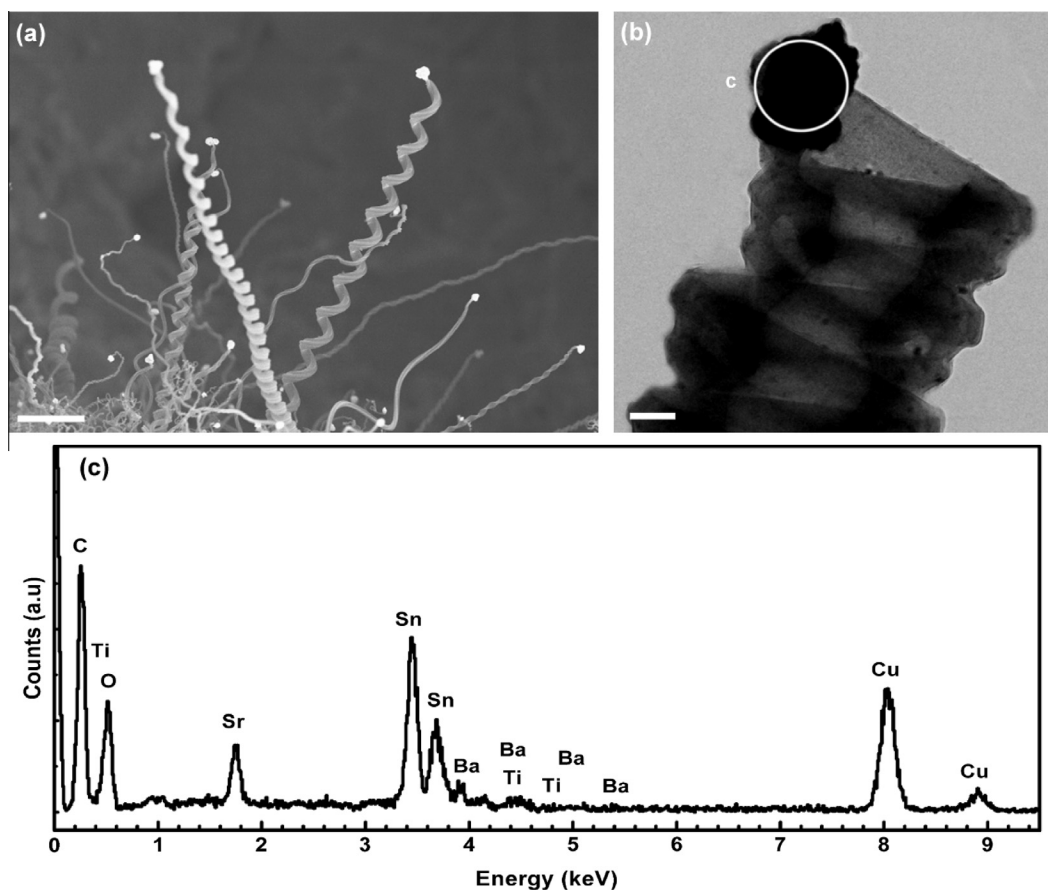
Fig. 3 – (a) Cross-sectional SEM view of CNCs grown on as-received BST substrates, showing the tip growth mode of CNCs. Scale bar: 3 μm. (b) TEM observation of an individual nanocoil, with a catalyst particle trapped at the tip. Scale bar: 100 nm. (c) Point-localized EDX spectrum of the catalyst particle, suggesting that the chemical composition of the catalyst is ∼BST with Sn decoration. The signal of Cu is attributed to the TEM grid.
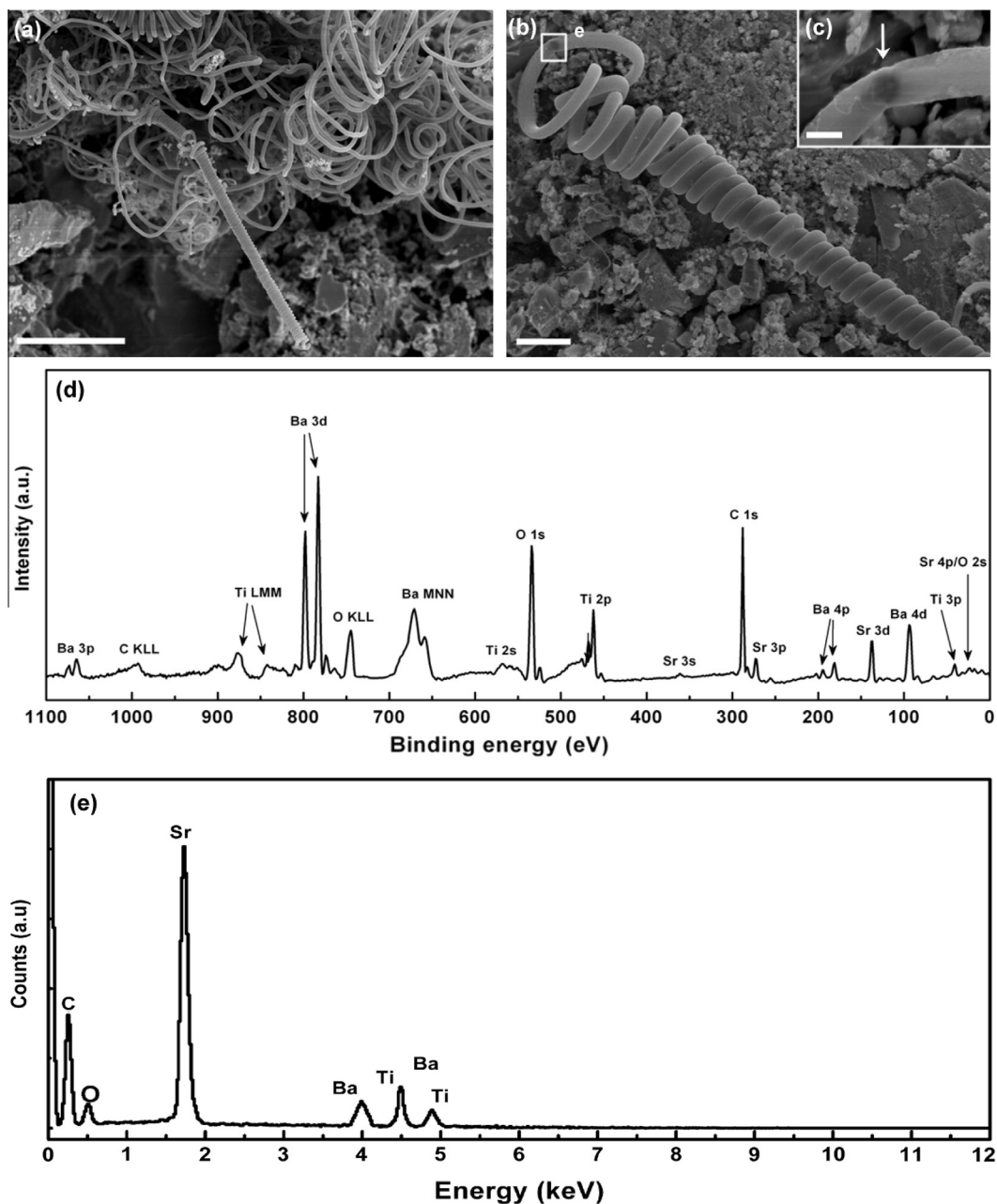
Fig. 4 – Investigations on the growth of CNCs on scratched BST substrates by metal-free C_2H_2-CVD (C_2H_2 flow rate: 40 sccm) at 750 °C. (a and b) SEM observations of solenoid-like CNCs. Scale bars: 3 μm. The inset shown in (c) indicates the presence of a catalyst particle (white arrow). Scale bar: 500 nm. (d) XPS spectrum and (e) EDX pattern (the white box marked in (b)) indicate the grown samples are free of metallic species.

this case, oxide asperities/nanoparticles with nanoscale curvatures on the surfaces may function as templates to tailor the nucleation of a carbon cap and the subsequent growth of 1D carbon nanomaterials, with or without the aid of any metal catalyst.

It is believed that the scratching of the BST substrate surface induced the formation of BST nanoparticles (NPs). It is likely that some of the NPs were in sizes and shapes suitable for the generation of helical carbon structures (Fig. 4c). The formation of CNCs in this case is attributed to the geometrical (particle shapes, facet orientations) and chemical (localized

compositions of distinct facets) faceting effects [7,16] of the BST NPs, which lead to uneven precipitation of carbons from different sites of the particles. As for the as-received substrate, there are freestanding BST NPs (coming off from the pit walls) inside the pits of the substrate, which act as reservoirs for the non-uniform dispersion of trapped Sn-residues onto these NPs. Under these circumstances, the carbon deposition/extrusion rates on different regions of the catalyst particle should be different, since they are dictated by this nonuniform distribution of Sn. Moreover, the BST NPs may synergistically have provided facet effects (facet geometry and

chemistry) on aiding the formation of CNCs. The helical growth of carbons is therefore achieved without the aid of any transition metal elements (Fe, Co, Ni *etc.*).

3.2. Synthesis of CNCs on BHF-etched BaSrTiO₃ substrates

3.2.1. Higher-yield production of CNCs

Using Sn and Fe to modify the BHF-etched BST substrates ($c(Sn^{2+})$ = 0.01 mol/L; $c(Fe^{2+})$ = 0.02 mol/L) is a further step toward catalyst design, which leads to more promising growth of CNCs (compared to that achieved on as-received substrates under identical CVD reaction conditions). Here the growth of CNCs not only occurs at the pits on the surface (similar to as-received samples), but also arises on the edges of the substrates. The synthesis was of such great efficiency that CNC

forests were grown. Fig. 5a displays the side-view SEM image of the grown CNC forests on the substrate edge. The overall thickness of the forest is about 30 μm. Fig. 5b provides a closer view of the CNC forest, the catalyst particles are found at the tips of the coils, suggesting that the CNCs grow *via* a tip growth mechanism. Apart from CNC forests, CNC bouquets also formed on the sample edges, as shown by the side-view SEM images in Fig. 5c and d. The SEM top-views shown in Fig. 5e and f present the growth of CNC clusters generated from the pits on the sample surface, where various shapes of nanocoils (twisted forms, solenoids, spring-like forms, waved fibers) can be observed.

3.2.2. Further characterization of CNCs and catalyst particles

Cross-sectional SEM observation of CNC forests at a higher magnification confirms that the CNC grow *via* tip growth, as displayed in Fig. 6a. TEM combined with point-localized EDX
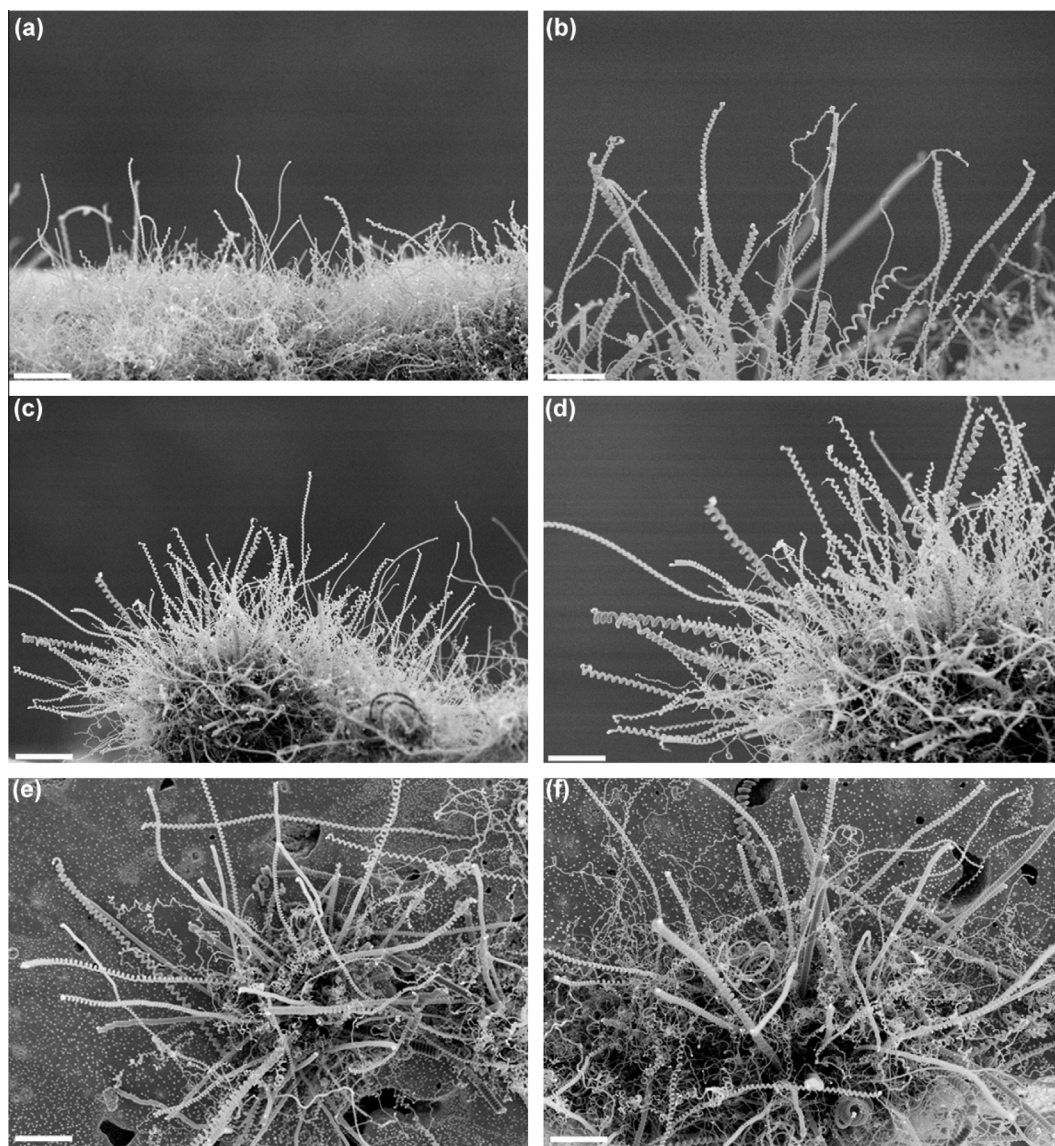
Fig. 5 – SEM view of CNCs grown on Sn-modified, BHF-etched BST substrates, showing (a and b) CNC forest grown on the sample edges, (c and d) CNC bouquet grown on the sample edges, and (e and f) CNC cluster grown from the sample surfaces. Scale bars: (a), (c), (e) 10 μm. (b), (d), (f) 5 μm.
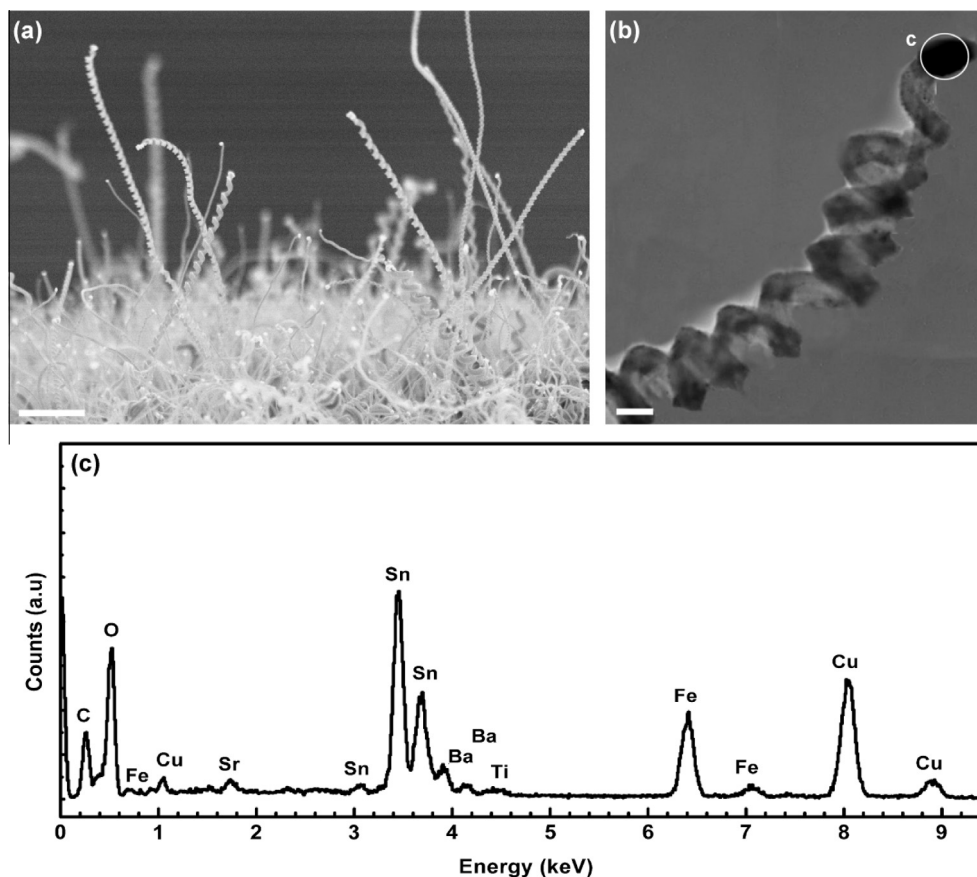
Fig. 6 – (a) Cross-sectional SEM view of CNCs grown on BHF-etched BST substrates, showing the tip growth mode of CNCs. Scale bar: 3 μm. (b) TEM image of an individual CNC with a catalyst particle located at the tip. Scale bar: 100 nm. (c) Point-localized EDX spectrum of the catalyst particle, indicating the presence of Sn and Fe. The signal of Cu is attributed to the TEM grid.

measurements were conducted to further examine the morphological structure of CNCs and detect the chemical constitution of the catalyst particles responsible for the coil growth, and is presented in Fig. 6b and c. Fig. 6b presents a spring-like CNC with a catalyst particle located at the tip. Point-localized EDX measurement (Fig. 6c) of the catalyst particle reveals that the catalyst NP contains Fe and Sn, with an estimated composition ratio (Fe/Sn) of 5:2, roughly consistent with the atomic ratio of elements used in the experiment (Fe/Sn: 2:1).

The investigations herein confirm that the elements of Fe and Sn are responsible for catalyzing the growth of CNCs, which is consistent with previous literature which claimed that Fe–Sn is catalytically active for inducing carbon helical structures. Moreover, the Fe and Sn ratio in the catalyst composition is an important factor for inducing non-linear growth. Wang et al. [12] observed that a Fe/Sn ratio of 4:1 can lead to the growth of coiled carbon nanowires. Chang et al. [24] suggested that a composition ratio of Fe and Sn (19:1) was critical to yield coiled carbon structures, by conducting CNC synthesis on stainless steel plates. Li and his colleagues [9] considered a Fe/Sn ratio of 15:6 optimal for the growth of coiled carbon nanostructures. Herein the EDX analysis of a catalyst particle located at the CNC tip shows the presence of Fe and Sn with a Fe/Sn ratio of approx. 5:2, which has been shown to be suitable for the growth of CNCs.

Furthermore, comparative studies have been performed by depositing either Fe or Sn separately on BST substrates and using them to grow carbon nanostructures under identical CVD conditions. Representative SEM images of the products (Fig. S5) reveal that while CNFs were grown on both samples, no CNCs were observed, indicating the importance of involving Fe–Sn binary catalysts for the formation of CNCs. The growth mechanism for the formation of CNCs is thought to be due to the difference between the carbon deposition/diffusion and extrusion rates in different regions of Fe–Sn binary catalyst particle. This may be as Fe and Sn carbides form within a catalyst particle during the CVD process, which might cause a difference in the extrusion speeds of the carbon network along different parts of the catalyst, as reported by Okazaki et al. [17] and by Li et al. [27].

3.2.3. Morphological control over the grown product

In this study tuning the amount of Sn used in catalyst precursor solutions ($c(Sn^{2+})$: 0.1, 0.06, 0.03, and 0.01 mol/L) or changing the C_2H_2 flow rate used during CVD reactions (40/20 sccm) leads to the morphological control over the grown product. Fig. 7 displays an SEM image library of various shapes of grown carbon nanostructures, dictated by the Sn^{2+} concentrations and C_2H_2 gas flow rate used. Fig. 7a and b show the formation of flower-like carbon structures, constituted by
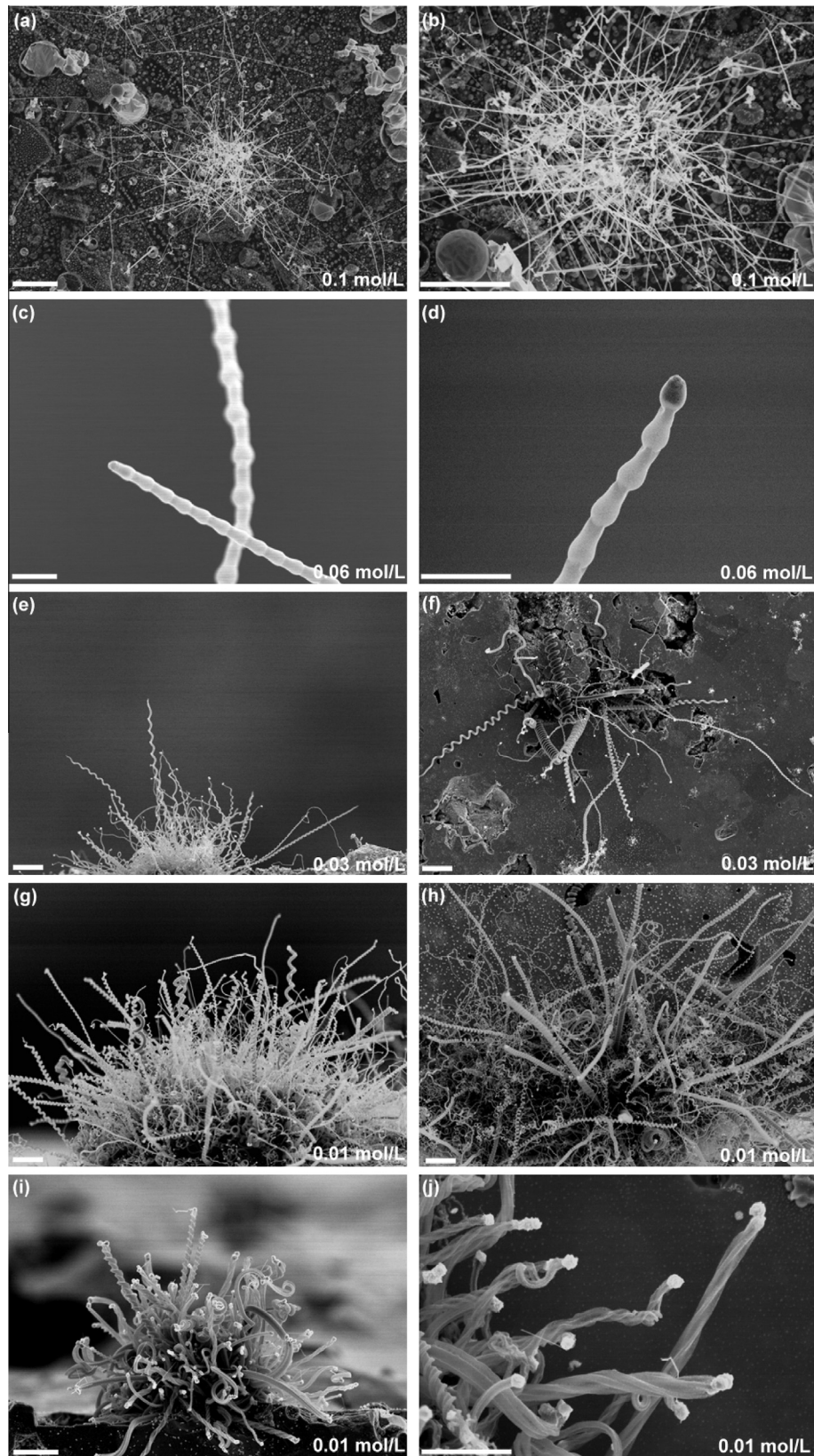
Fig. 7 – SEM image library of the effect of Sn concentration and C₂H₂ flow rate used on the morphologies of the grown product, showing carbon nanostructures with distinct shapes: (a and b) flower-like structures constituted by straight CNFs, (c and d) beaded CNFs, (e and f) CNCs, (g and h) CNCs (with higher yield), and (i and j) twisted tubules. Scale bars: 3 μm. The amount of Sn used in each case during substrate preparation is marked on each image.

straight CNFs, where the substrate was coated with a solution of 0.1 mol/L Sn^{2+} in ethanol, no coiled carbon nanostructures were observed in this experiment. Once the concentration of Sn^{2+} is reduced to 0.06 mol/L, beaded CNFs start to dominate the morphologies of grown products (Fig. 7c and d). Further reducing the amount of Sn triggers carbon helical growth. Fig. 7e and f present the formation of CNCs on the edge as well as on the flat surface of the substrate, when the concentration of Sn^{2+} is approx. at 0.03 mol/L. Furthermore, a coating of Sn^{2+} solution with concentration at 0.01 mol/L for sample treatments results in encouraging production of CNCs, as shown in Fig. 7g and h. However, the morphologies of carbon helical structures can be changed from CNCs to CNC–CNF hybrid structures or twisted carbon tubules (Fig. 7i and j), when the C_2H_2 gas flow rate was decreased from 40 sccm to 20 sccm at growth.

4. Discussion

The results presented above feature a simple method for Sn-assisted synthesis of helical carbon nanostructures of good quality on BST substrates. A highlight of these results is the synthesis of CNC forests. Firstly, it is instructive to compare the growth results that have been achieved in this study with those grown on other catalyst systems involving the use of Sn, as there is no previous study on the growth of CNC on BST substrates. For Sn-involved cases, there are numerous reports indicating that Sn is effective for inducing coiled carbon nanotube growth; whether as co-catalyst with transition metals such as Fe [9,11,12,17], Ni [24,25], and Cr [24,25], in its oxidized form (SnO_2) [26] or in carbide form ($Fe_3C(Sn)$) [27]. For instance, Wang et al. [12] demonstrated the synthesis of coiled carbon nanowires with the aid of a Fe and Sn bi-metallic catalyst. A specific model based on the mutual solubility of Fe and Sn, along with metallic catalyst–carbon product interactions, has been proposed in their study to elucidate the role of the Sn. Similarly, the yield and quality of carbon helices synthesized in this study have been greatly enhanced by the involvement of Sn, although the exact chemical composition of the catalyst particles at the growth stage remains unknown.

The use of helical carbons in real applications strictly depends upon the ability to tailor the morphologies and shapes of these nanomaterials. In typical CVD reactions, the synthesis of carbon nanomaterials can be controlled by varying growth temperature, ambient gas, carbon feedstock, and the type of catalyst. The work presented here demonstrates simple synthetic methods to achieve structural control over the grown carbon products by varying the concentrations of Sn-coating on BHF-etched BST substrates or flow rates of C_2H_2 during the CVD processes. As for tuning the Sn concentrations used in the fabrication of the catalyst precursors, large Sn doses (0.1 mol/L) lead to the formation of straight CNFs (Fig. 7a–b), whilst small concentrations (0.01–0.03 mol/L) of Sn give rise to non-linear growth of carbons (Fig. 7e–j). The largest quantity of CNCs was obtained when the amount of Sn used was 0.01 mol/L (Fig. 7g and h). The reason for these scenarios is suggested to be the non-uniform distribution of Fe and Sn within the catalyst particles leading to the

difference in carbon extrusion rates in different parts of the catalyst, where the small doses of Sn cause large gradients of Sn concentrations within catalysts, resulting in asymmetric geometry and chemistry of the catalyst particles. A sketch model of such an asymmetric catalyst particle is depicted in Fig. 8 (adapted from Ref. [28]) to explain the observed phenomenon. As for altering the C_2H_2 gas flow rates during CVD processes, it can be clearly seen in our investigation that an apparent morphological change of helical carbon nanostructures (from nanocoils (Fig. 7g) to twisted tubules (Fig. 7i)) occurred, when the C_2H_2 gas flow rate was varied from 40 sccm to 20 sccm during synthesis. This observation suggests that the C_2H_2 gas (concentration, pressure etc.) might be capable of dynamic restructuring of the catalyst particles at CNC growth, which have been observed recently by using Cu as a CNC growth catalyst [7,8,29].

In this study, two types of BST substrates have been employed for investigating the synthesis of CNCs on them: as-received substrates (BST-Sn) and prepared BHF-etched BST substrates (Fe–Sn). It was subsequently found that both Sn-decorated BST oxide NPs and Sn-modified Fe metallic nanopowders can lead to the formation of CNCs. Also, 1D helical carbon fibers can be obtained on scratched BST substrates from metal-free CVD reactions. Comparisons between the differences of grown CNC products on these two different substrates are depicted in Table 1.

This study demonstrates that introducing Sn into the catalyst systems (either perovskite oxides or metals) induces the helical growth of carbons, although the roles of Sn in aiding the CNC growth differ one from the other. Our findings are important because it extends our discussions to a broader context as to 'whether CNCs can be formed from any Sn coated substrates?' It is well known that Sn has a non-wetting interaction with graphite thus could promote helical growth of carbons [12]. With regard to metals (Fe, Ni, Cr, Mn etc.), there have already been quite a few reports on answering this question. It has been proposed that the formation of
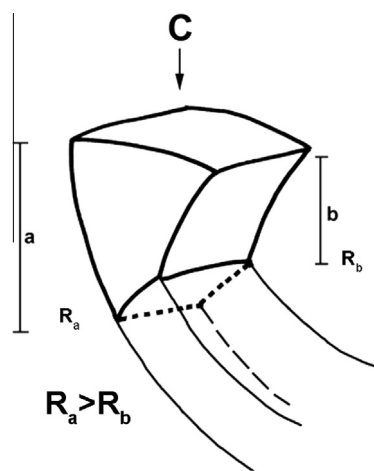
Fig. 8 – A sketched model of hypothetical growth mechanism of CNCs showing a non-uniform catalyst particle. The C is extruded at different rates (R_a, R_b) due to the asymmetric geometry and chemistry of the particle, inducing the coiling during carbon fiber growth (adapted from Ref. [28]).

Table 1 – Comparison of CNCs grown on different BST substrates (identical CVD conditions).

Samples	Positions of grown CNCs	Product: selectivity to CNCs	SEM: product morphology	EDX: catalyst materials	Raman G/D ratio
As-received	Pits	91%	CNC clusters	Sn-decorated BST NPs	2.2
BHF-etched	Pits and edges	97%	CNC forests	Fe–Sn binary NPs	3.4
Scratched	Sample surfaces	14%	CNC individuals	BST NPs (metal-free)	1.4

bimetallic phases (e.g. Fe–Sn mixtures) or complex alloys (e.g. Fe–Ni–Cr–Sn) gives rise to non-uniform distributions of Sn within the catalyst particles, which can lead to the uneven deposition/extrusion of carbons to establish the helical growth. With regard to oxides, however, we stress that the possibility of growing CNCs from a Sn/oxide nanocomposite relies on the growth mode adopted by Sn when making contact with the oxide substrate. As for our BST case, it is expected that Sn will wet the BST surface, because Sn has a substantially lower surface energy (approx. 0.5–0.7 J/m^2) [30] when compared to BST (approx. 1.5–2.0 J/m^2) [31,32]. During the CVD process, Sn (in the liquid state) will wet the irregularly-shaped BST polyhedral NPs and this leads to carbon coil growth *via* the mechanism shown in Fig. 8 [28]. For future studies of this type, it would be interesting to use SiO$_2$ particles because Sn will not wet SiO$_2$ [33], and hence if our proposed mechanism is correct then it will not be possible to generate helical growth of carbon with Sn-decorated SiO$_2$ NPs.

5. Conclusions

We developed a new way to grow high-quality CNC forests (about 30 μm thick) on polycrystalline BST substrates by using Sn-assisted, C$_2$H$_2$-CVD at 750 °C. We also demonstrated structural control over the carbon product by simply altering the Sn concentrations used in catalyst precursors or C$_2$H$_2$ flow rates used in CVD reactions. We suggested a convenient method to introduce Sn into the catalyst system and showed that Sn played an important role in the formation of CNCs by cooperating with either perovskite oxides (BST) or transition metals (Fe). We proposed a growth model based on different carbon extrusion rates from different regions of the catalyst NPs due to the asymmetric geometry and chemistry of the Sn-modified particle, therefore inducing the coiling during fiber growth. Furthermore, the catalytic roles of Sn played in CNC synthesis have been discussed in a wider context. Future work will focus on the synthesis of more uniform CNCs (similar coil diameters, lengths and shapes) with the aid of more homogeneous catalyst particles (similar sizes and chemical compositions), in conjunction with other catalyst preparation methods (such as sol–gel, electrospray) and CNT reaction protocols (aerosol-CVD). Our study might not only pave the way towards designing new catalyst systems for efficient synthesis of helical carbon nanostructures, but also herald the beginning of a new age of perovskite-based nanoelectronic devices.

Appendix A. Supplementary data

Supplementary data associated with this article can be found, in the online version, at http://dx.doi.org/10.1016/j.carbon. 2013.03.027.

REFERENCES

[1] Hanus MJ, Harris AI. Synthesis, characterisation and applications of coiled carbon nanotubes. J Nanosci Nanotechnol 2010;10(4):2261–83.

[2] Zhang M, Li J. Carbon nanotube in different shapes. Mater Today 2009;12(6):12–8.

[3] Chen XQ, Zhang SL, Dikin DA, Ding WQ, Ruoff RS, Pan LJ, et al. Mechanics of a carbon nanocoil. Nano Lett 2003;3(9):1299–304.

[4] Liu WC, Lin HK, Chen YL, Lee CY, Chiu HT. Growth of carbon nanocoils from K and Ag cooperative bicatalyst assisted thermal decomposition of acetylene. Acs Nano 2010;4(7):4149–57.

[5] Zhang ZJ, He PG, Sun Z, Feng T, Chen YW, Li HL, et al. Growth and field emission property of coiled carbon nanostructure using copper as catalyst. Appl Surf Sci 2010;256(14):4417–22.

[6] Tang NJ, Wen JF, Zhang Y, Liu FX, Lin KJ, Du YW. Helical carbon nanotubes: catalytic particle size-dependent growth and magnetic properties. Acs Nano 2010;4(1):241–50.

[7] Jian X, Jiang M, Zhou ZW, Yang ML, Lu J, Hu SC, et al. Preparation of high purity helical carbon nanofibers by the catalytic decomposition of acetylene and their growth mechanism. Carbon 2010;48(15):4535–41.

[8] Shaikjee A, Franklyn PJ, Coville NJ. The use of transmission electron microscopy tomography to correlate copper catalyst particle morphology with carbon fiber morphology. Carbon 2011;49(9):2950–9.

[9] Li DW, Pan LJ, Liu DP, Yu NS. Relationship between geometric structures of catalyst particles and growth of carbon nanocoils. Chem Vapor Depos 2010;16(4–6):166–9.

[10] Liu Q, Cui Z-M, Ma Z, Bian S-W, Song W-G. Carbon materials with unusual morphologies and their formation mechanism. J Phys Chem C 2007;111(33):12420–4.

[11] Kanada R, Pan L, Akita S, Okazaki N, Hirahara K, Nakayama Y. Synthesis of multiwalled carbon nanocoils using codeposited thin film of Fe–Sn as catalyst. Jpn J Appl Phys 2008;47(4):1949–51.

[12] Wang W, Yang K, Gaillard J, Bandaru PR, Rao AM. Rational synthesis of helically coiled carbon nanowires and nanotubes through the use of tin and indium catalysts. Adv Mater 2008;20(1):179–82.

[13] Bandaru PR, Daraio C, Yang K, Rao AM. A plausible mechanism for the evolution of helical forms in

nanostructure growth. J Appl Phys 2007;101(9):0943071–943074.

[14] Yang S, Chen X, Kikuchi N, Motojima S. Catalytic effects of various metal carbides and Ti compounds for the growth of carbon nanocoils. Mater Lett 2008;62(10–11):1462–5.

[15] Qi XS, Zhong W, Yao XJ, Zhang H, Ding Q, Wu Q, et al. Controllable and large-scale synthesis of metal-free carbon nanofibers and carbon nanocoils over water-soluble Na_x–K_y catalysts. Carbon 2012;50(2):646–58.

[16] Xia JH, Jiang X, Jia CL, Dong C. Hexahedral nanocementites catalyzing the growth of carbon nanohelices. Appl Phys Lett 2008;92(6):0631211–631213.

[17] Okazaki N, Hosokawa S, Goto T, Nakayama Y. Synthesis of carbon tubule nanocoils using Fe–In–Sn–O fine particles as catalysts. J Phys Chem B 2005;109(37):17366–71.

[18] Li DW, Pan LJ, Qian JJ, Liu DP. Highly efficient synthesis of carbon nanocoils by catalyst particles prepared by a sol–gel method. Carbon 2010;48(1):170–5.

[19] Daraio C, Nesterenko VF, Jin S, Wang W, Rao AM. Impact response by a foamlike forest of coiled carbon nanotubes. J Appl Phys 2006;100(6):0643091–643094.

[20] Im J, Auciello O, Streiffer SK. Layered barium strontium titanate thin films for high frequency tunable devices. Thin Solid Films 2002;413(1–2):243–7.

[21] Mendoza F, Kumar A, Martinez R, Scott JF, Weiner B, Katiyar RS, et al. Conformal coating of ferroelectric oxides on carbon nanotubes. Europhys Lett 2012;97(2):270011–5.

[22] Kawasaki M, Takahashi K, Maeda T, Tsuchiya R, Shinohara M, Ishiyama O, et al. Atomic control of the strontium titanate crystal surface. Science 1994;266(5190):1540–2.

[23] Li DW, Pan LJ. Growth of carbon nanocoils using Fe–Sn–O catalyst film prepared by a spin-coating method. J Mater Res 2011;26(16):2024–32.

[24] Chang NK, Chang SH. High-yield synthesis of carbon nanocoils on stainless steel. Carbon 2008;46(7):1106–9.

[25] Su CC, Chang SH. Radial growth of carbon nanocoils on stainless steel wires coated with tin particles using chemical vapor deposition from acetylene. Mater Lett 2011;65(7):1114–6.

[26] Wang L, Li C, Gu F, Zhang C. Facile flame synthesis and electrochemical properties of carbon nanocoils. J Alloys Compd 2009;473(1–2):351–5.

[27] Li D, Pan L, Wu Y, Peng W. The effect of changes in synthesis temperature and acetylene supply on the morphology of carbon nanocoils. Carbon 2012;50(7):2571–80.

[28] Grobert N. Novel carbon nanostructures. University of Sussex, PhD thesis, 2000.

[29] Jian X, Jiang M, Zhou Z, Zeng Q, Lu J, Wang D, et al. Gas-induced formation of cu nanoparticle as catalyst for high-purity straight and helical carbon nanofibers. Acs Nano 2012;6(10):8611–9.

[30] Yuan ZF, Mukai K, Takagi K, Ohtaka M, Huang WL, Liu QS. Surface tension and its temperature coefficient of molten tin determined with the sessile drop method at different oxygen partial pressures. J Colloid Interface Sci 2002;254(2):338–45.

[31] Somorjai GA. Chemistry in Two Dimensions: Surfaces. Cornell University Press; 1981.

[32] Tu K, Mayer JW, Feldman LC. Electronic Thin Film Science: For Electrical Engineers and Materials Scientists. Macmillan; 1992.

[33] Chen PJ, Colaianni ML, Yates JT, Arbab M. Thermal properties of the tin/silica interface as studied by surface spectroscopies. J Non-Cryst Solids 1993;155(2):131–40.